International Journal of Control, Automation, and Systems VV(X) (YYYY) 1-8
http://dx.doi.org/10.1007/s12555-xxx-xxxx-x
ISSN:1598-6446 eISSN:2005-4092
http://www.springer.com/12555

VALINOR: a lightweight leg inertial odometry for humanoid robots

Arnaud Demont*, Mehdi Benallegue, Thomas Duvinage, and Abdelaziz Benallegue

Abstract: This article describes the preparation procedure for publication in the International Journal of Control, Automation, and Systems (IJCAS), and this template applies both for initial submission and the final camera-ready manuscript of the paper. When authors submit their work for review, it is necessary to follow these instructions. The abstract should not exceed 300 words for regular papers or 75 words for technical notes and correspondence without equations, references, and footnotes.

Keywords: Legged robots, proprioceptive odometry, state estimation, tilt estimation.

1. INTRODUCTION

Humanoid robot navigation in real-world environments remains a core challenge in robotics. For robots to be deployed at scale in society and industry, whether in healthcare facilities or warehouses, they must operate robustly in dynamic, unstructured, and human-centric environments [1]. This requires strong guarantees on their ability to plan motion, and execute actions in real time. In comparison to other legged robots, the control of humanoids is particularly difficult due to their complex underactuated dynamics controlled through contact with the environment [2]. Their control must therefore be as theoretically grounded as possible, in order to ensure safe, predictable, and certifiable behavior [3] pas citer celui la.

In the meantime, methods for motion generation continue to gain in complexity and capability. Notably, Model Predictive Control (MPC) [4–6], reinforcement learning-based controllers [7, 8], and foundation models [9, 10] are becoming more prevalent due to their ability to handle long-horizon planning, complex dynamics, and to their versatility. However, these advances come at the cost of increased computational complexity, running them in real-time on resource-limited platforms like drones or embedded systems thus becomes challenging [11–14]. Since the control part is getting heavier, one practical solution is to reduce the computational load of other parts of the pipeline. The state estimation part is one of its cornerstone of the pipeline, since other components depend on its output and must wait for it before executing, preventing parallelization. It is therefore especially critical to try and reduce the computation time of the state estimation part.

State estimation for legged robots has also known notable improvements in the past years, the main trend aiming towards improving its global accuracy by incorporating additional sensors to the commonly used sensors (IMU, joint encoders, force sensors, etc.), especially exteroceptive sensors, such as cameras, LiDARs, etc. [15–17]. Such methods show remarkable accuracies. However, they also tend to be more and more computationally expensive (order of the millisecond [17]).

For this reason, there is still a need for lightweight state estimation methods, which rather than adding new sensors, focus on improving the estimation of key variables at high frequency using the proprioceptive sensors readily available on the robot. What might be the biggest "recent" breakthrough among proprioceptive state estimation methods is the use of contact information to perform legged odometry (also called "Leg" odometry) [18]: assuming no slippage, contacts are considered fixed points in the environment, providing a measurement of the robot's kinematics in the world using joint encoders. Fusing the usual Inertial odometry with this method prevents the position from drifting due to the integration of IMU's signal noise, and provides the observability of the robot's tilt and velocity [19–22]. Indeed, until then, a commonly used method for tilt estimation was to consider the linear acceleration negligible with respect to the gravitational acceleration (e.g. [23]). However, estimation degrades when the assumption of no contact slippage is violated, and legged odometry relies on the accuracy of the estimated pose of the contact at the time it is considered fixed [24, 25]. Work has thus been done to address the problem of contact slippage, for example by discarding unreliable contacts [24–26], or by attempting to correct the contact reference position [19, 27, 28]. While it has

A. Demont, M. Benallegue and A. Benallegue are with the CNRS-AIST JRL (Joint Robotics Laboratory), IRL, National Institute of Advanced Industrial Science and Technology (AIST), 1-1-1 Umezono, Tsukuba, Ibaraki 305-8560 Japan.
A. Demont and A. Benallegue are also with Université Paris-Saclay, 3 rue Joliot Curie, Bâtiment Breguet, 91190 Gif-sur-Yvette, France, and Laboratoire d'Ingénierie des Systèmes de Versailles, 10-12 avenue de l'Europe, 78140 Vélizy, France.
e-mails: arnaud.demont@aist.go.jp, mehdi.benallegue@aist.go.jp, abdelaziz.benallegue@uvsq.fr.
* Corresponding author.

been proven that using proprioceptive sensors, the position and the yaw orientation of the robot in the world frame remain non-observable [19], methods exploiting them have proven to be more than enough in concrete use-cases when the pose needs to be reliable only locally, like for remotely controlled robots [29] or when task planning is also made in the robot's local environment [30].

In this work we propose VALINOR, a method for Leg-Inertial odometry for legged robots, which relies on a highly accurate tilt estimate provided by a complementary filter [22]. This complementary filter allows for a much faster computation than the conventionally used Kalman Filter (e.g. [27]), and offers mathematical convergence guarantees on the tilt and linear velocity estimate. We show that VALINOR achieves estimation accuracy on par with state-of-the-art methods, aligning with our objective of lightweight yet accurate and certifiable state estimation.

1.1. Contributions

- Presentation of axis-agnostic orientation combinations.
- Lightweight combination of Leg Odometry with a highly accurate tilt estimate.
- Experimental evaluation of the Tilt Observer.
- The code of the Tilt Observer is open source[1], as well as a ROS wrapper[2].

2. PRELIMINARIES

2.1. General notations

- The general notation for kinematic variables is ${}^{1}\bigcirc_{2}$, expressing the kinematics of the frame 2 in the frame 1. To simplify the notation, kinematics in the world frame are written without the $\mathcal{W}$ symbol: ${}^{\mathcal{W}}\bigcirc_{2} = \bigcirc_{2}$.
- We define $\boldsymbol{\Omega}$ the function that associates the rotation matrix to the corresponding rotation vector:

$$\mathrm{SO}(3) \to \mathbb{R}^3 \tag{1}$$

$$\boldsymbol{\Omega} : \boldsymbol{R} \mapsto \boldsymbol{v}, \quad \text{s.t.} \quad \exp(\mathrm{S}(\boldsymbol{v})) = \boldsymbol{R} \text{ and } |\boldsymbol{v}| \leq \boldsymbol{\pi} \tag{2}$$

- $[.]_\times$ is the skew-symmetric operator.
- Define here the tilt?
- Define vec
- The world frame and the robot's IMU frame are denoted $\mathcal{W}$ and $\mathcal{I}$, respectively. The frame associated with the i-th contact is denoted $\mathcal{C}_i$. The anchor point, defined in Section 4, is denoted $\mathcal{A}$.
- We define n_c the number of current contacts set with the environment.

[1] https://github.com/ArnaudDmt/state-observation

[2] https://github.com/ArnaudDmt/state_observation_ros.git

3. AXIS-AGNOSTIC ORIENTATION COMBINATIONS

In this Section, we introduce the concept of *axis-agnostic* orientation representation. This answers the need for a representation that would allow for the combination of orientations, without axis ambiguities.

3.1. Tilt and yaw representation

3.2. Rotation matrix to yaw agnostic Useless here?

Rotation matrix to yaw axis agnostic:

$$\theta = \mathrm{atan2}\left(\boldsymbol{v}_x \cdot \tilde{\boldsymbol{v}}_y - \boldsymbol{v}_y \cdot \tilde{\boldsymbol{v}}_x,\ \boldsymbol{v}_x \cdot \tilde{\boldsymbol{v}}_x + \boldsymbol{v}_y \cdot \tilde{\boldsymbol{v}}_y\right) \tag{3}$$

where $v = \begin{bmatrix} R_{3,2} \\ -R_{3,1} \\ 0 \end{bmatrix}$ is the invariant horizontal vector projected onto the XY-plane $\in \mathbb{R}^2$ and $\tilde{v} = R_{2\times 2} \cdot v$

3.3. Merge tilt + yaw axis agnostic

Let us consider two rotation matrices $\boldsymbol{R}_1$ and $\boldsymbol{R}_2$, corresponding to the orientations of the frames 1 and 2. The objective is to merge the *tilt* of the frame 1 with the *yaw* of the frame 2.

First, we compute the projection of $\boldsymbol{tilt}_1$ in the frame 2:

$$\begin{bmatrix} v_x \\ v_y \\ v_z \end{bmatrix} = \boldsymbol{R}_2 \cdot \boldsymbol{tilt}_1 \tag{4}$$

This allows us to compute the invariant orthogonal vector $\boldsymbol{m}$:

$$\boldsymbol{m} = \begin{cases} \begin{bmatrix} 1 \\ 0 \\ 0 \end{bmatrix}, & \text{if } \left\| \begin{bmatrix} v_x \\ v_y \end{bmatrix} \right\| \approx 0 \\ \frac{1}{\sqrt{v_x^2 + v_y^2}} \begin{bmatrix} v_y \\ -v_x \\ 0 \end{bmatrix}, & \text{otherwise} \end{cases} \tag{5}$$

We then project $\boldsymbol{m}$ in the frame 2:

$$\boldsymbol{m}_2 = \boldsymbol{R}_2^T \boldsymbol{m}. \tag{6}$$

We finally obtain a rotation matrix $\boldsymbol{R}$, resulting from the combination of the tilt of the frame 1 and of the yaw of the frame 2:

$$\boldsymbol{R} = \begin{pmatrix} \frac{\boldsymbol{m}\times\boldsymbol{e}_z}{\|\boldsymbol{m}\times\boldsymbol{e}_z\|} & \frac{\boldsymbol{e}_z\times\boldsymbol{m}\times\boldsymbol{e}_z}{\|\boldsymbol{m}\times\boldsymbol{e}_z\|} & \boldsymbol{e}_z \end{pmatrix} \cdot \begin{pmatrix} \frac{\boldsymbol{m}_2\times\boldsymbol{tilt}_1}{\|\boldsymbol{m}_2\times\boldsymbol{tilt}_1\|} & \frac{\boldsymbol{tilt}_1\times\boldsymbol{m}_2\times\boldsymbol{tilt}_1}{\|\boldsymbol{m}_2\times\boldsymbol{tilt}_1\|} & \boldsymbol{tilt}_1 \end{pmatrix}^T \tag{7}$$

4. DEFINITION OF THE ANCHOR POINT

We define here the notion of anchor point, since it will be used extensively in the following sections. The anchor point, denoted $\mathcal{A}$, is a point attached to the robot, and which is considered to have a zero velocity in the world frame. As will be explained in Section 5.2, this frame is especially important, since it provides a measurement of the robot's IMU velocity in the world frame. In the case of legged robots, it is common to assume that contacts with the environment are fixed. Any point of a contact surface would thus be usable as an anchor point. However, we need a unique point that remains valid as contacts are created and broken, and which respects as best as possible the zero-velocity criterion. We thus compute its kinematics through a weighted average of the kinematics of the current contacts, as shown in Figure 1.

The weighting coefficients are defined such that weaker contacts, which are prone to violate Coulomb's inequality and thus to slip, contribute less to the anchor point's kinematics computation. Given mg the weight of the robot, we first compute

$$u_i = \frac{\boldsymbol{F}_{i,z}}{\sqrt{\boldsymbol{F}_{i,x}^2 + \boldsymbol{F}_{i,y}^2} + \varepsilon mg}, \tag{8}$$

the ratio of the normal force to the tangential force[3] at the contact i. The contact's weighting coefficient λ_i is then:

$$\lambda_i = \frac{u_i}{\sum_{j=1}^{n_c} u_i}. \tag{9}$$

It is important to note that although the anchor point is defined to have zero velocity in the world, its pose may still evolve over time. In discrete time, it has zero velocity? Maybe such a definition helps getting rid of the additional frame which coincides with it.

Based on this definition, we give the position and linear velocity of the anchor point in the IMU's frame:

$${}^{\mathcal{I}}\boldsymbol{p}_{\mathcal{A}} = \sum_{i}^{n_c} \lambda_i {}^{\mathcal{I}}\boldsymbol{p}_{\mathcal{C}_i}, \tag{10}$$

$${}^{\mathcal{I}}\dot{\boldsymbol{p}}_{\mathcal{A}'} = \sum_{i}^{n_c} \lambda_i {}^{\mathcal{I}}\dot{\boldsymbol{p}}_{\mathcal{C}_i}, \tag{11}$$

with ${}^{\mathcal{I}}\boldsymbol{p}_{\mathcal{C}_i}$ the position and ${}^{\mathcal{I}}\dot{\boldsymbol{p}}_{\mathcal{C}_i}$ the linear velocity of the i-th contact in the IMU's frame, which are directly provided by the robot's joint encoders and geometrical model.

TODO

5. TILT OBSERVER WITH PROOF OF CONVERGENCE

The proposed estimator relies on a highly accurate estimate of the IMU's tilt provided by a complementary filter, introduced in [22], which we will call *Tilt Observer*.

[3]The term ε, arbitrarily small, allows to deal with the case where the tangential force is zero.

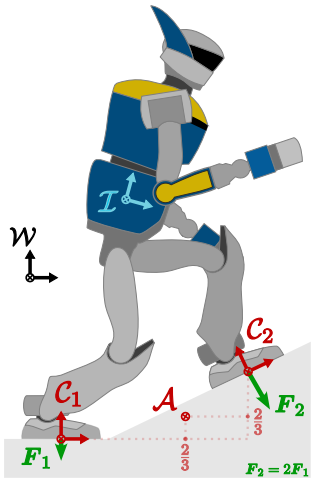

Fig. 1. Illustration of the anchor point position computation and of the reference frames used in VALINOR. $\mathcal{W}$: world frame; $\mathcal{I}$: IMU frame; $\mathcal{C}_i$: frame of the i-th contact. For clarity, only the weighted average of the contact positions is shown. In this example, $\boldsymbol{F}_2 = 2\boldsymbol{F}_1$ and so $\lambda_2 = \frac{2}{3}$.

Fig. 2. Tilt

5.1. Definition of the State Variables

The Tilt Observer is able to provide estimates of the following two variables:

- $\boldsymbol{v}_{\mathcal{I},l} \triangleq \boldsymbol{R}_{\mathcal{I}}^T \boldsymbol{v}_{\mathcal{I}}$ the linear velocity of the IMU's frame in the world frame, expressed in the frame of the IMU.
- $\boldsymbol{R}_{\mathcal{I}}^T \boldsymbol{e}_z$ the tilt of the IMU.

We thus define the state variables:

$$\boldsymbol{x}_1 \triangleq \boldsymbol{v}_{\mathcal{I},l} \quad , \boldsymbol{x}_1 \in \mathbb{R}^3, \tag{12}$$

$$\boldsymbol{x}_2 \triangleq \boldsymbol{R}_{\mathcal{I}}^T \boldsymbol{e}_z \quad , \boldsymbol{x}_2 \in \mathbb{S}^2. \tag{13}$$

The set $\mathbb{S}^2 \subset \mathbb{R}^3$ is the unit sphere centered at the origin, and defined as

$$\mathbb{S}^2 = \left\{ \boldsymbol{x} \in \mathbb{R}^3 \middle| \|\boldsymbol{x}\| = 1 \right\} \tag{14}$$

This figure is uncited

5.2. Definition of the Measurements

The measurements required by the Tilt Observer are:

- $\boldsymbol{y}_g$ the signal of the IMU's gyrometer.

- $\boldsymbol{y}_a$ the signal of the IMU's accelerometer.
- $\boldsymbol{y}_v$ a measurement of $\boldsymbol{v}_{\mathcal{I},l}$.

Since no sensor provides a direct measurement of $\boldsymbol{v}_{\mathcal{I},l}$, we obtain $\boldsymbol{y}_v$ from an intermediate zero-velocity pseudo-measurement of the anchor point $\mathcal{A}$ in the world, giving:

$$\boldsymbol{y}_v = -[\boldsymbol{y}_g]_\times {}^{\mathcal{I}}\boldsymbol{p}_{\mathcal{A}} - {}^{\mathcal{I}}\dot{\boldsymbol{p}}_{\mathcal{A}} \tag{15}$$

${}^{\mathcal{I}}\boldsymbol{p}_{\mathcal{A}}$ and ${}^{\mathcal{I}}\dot{\boldsymbol{p}}_{\mathcal{A}}$ are the position and linear velocity of the anchor point in the IMU's frame, obtained using(10) and (11).

5.3. Definition of the Filter

As explained in Cite, the state dynamics of our system can be written:

$$\dot{\boldsymbol{x}}_1 = -[\boldsymbol{y}_g]_\times \boldsymbol{x}_1 - g_0 \boldsymbol{x}_2 + \boldsymbol{y}_a, \tag{16}$$
$$\dot{\boldsymbol{x}}_2 = -[\boldsymbol{y}_g]_\times \boldsymbol{x}_2. \tag{17}$$

We can then write a complementary filter which uses the system's dynamics as a feed-forward, and corrects the estimated state using the velocity measurement $\boldsymbol{y}_v$:

$$\dot{\hat{\boldsymbol{x}}}_1 = -[\boldsymbol{y}_g]_\times \hat{\boldsymbol{x}}_1 - g_0 \hat{\boldsymbol{x}}'_2 + \boldsymbol{y}_a + \alpha_1 (\boldsymbol{y}_v - \hat{\boldsymbol{x}}_1), \tag{18}$$
$$\dot{\hat{\boldsymbol{x}}}'_2 = -[\boldsymbol{y}_g]_\times \hat{\boldsymbol{x}}_2 - \frac{\alpha_2}{g_0}(\boldsymbol{y}_v - \hat{\boldsymbol{x}}_1), \tag{19}$$
$$\dot{\hat{\boldsymbol{x}}}_2 = -\left[\boldsymbol{y}_g - \gamma [\hat{\boldsymbol{x}}_2]_\times \hat{\boldsymbol{x}}'_2\right]_\times \hat{\boldsymbol{x}}_2. \tag{20}$$

α_1, α_2 and γ are positive scalar gains. $\hat{\boldsymbol{x}}_1$ and $\hat{\boldsymbol{x}}_2$ are estimates of $\boldsymbol{x}_1$ and $\boldsymbol{x}_2$, respectively.

The particularity of the Tilt Observer, in comparison to similar complementary filters (e.g. [31]), is the use of an intermediate estimate of the tilt, denoted $\hat{\boldsymbol{x}}'_2$. This intermediate variable allows for a fast convergence of $\hat{\boldsymbol{x}}_2$, while making sure it remains on the unit sphere.

5.4. Advantages of the Tilt Observer

The use of a complementary filter for the Tilt Observer presents notable strengths in comparison to other methods like the commonly used Kalman Filter. First, it allows us to work in the frequency domain. This is particularly suitable for our model since the assumption of fixed contacts used to obtain the velocity measurement $\boldsymbol{y}_v$ is more valid in low frequency than in high frequency. In (16), we thus use the IMU measurements for the high frequency variation of $\hat{\boldsymbol{x}}_1$, and $\boldsymbol{y}_v$ for its low frequency variation. Second, one iteration of the filter only consists in computing three equations, it also doesn't involve any matrix inversion and is thus extremely computationally cheap, as will be shown in Section 7.3. Finally, the formulation as a complementary filter allows to conduct a convergence analysis of the estimation error, providing strong mathematical guarantees on the estimator's performances. Especially here, it has been shown in [22] that:

- The dynamics of the estimation error is autonomous, and thus does not depend on the state.
- The intermediate estimator $\{\hat{\boldsymbol{x}}_1, \hat{\boldsymbol{x}}'_2\}$ is *globally exponentially stable*, with respect to the origin $(0,0)$.
- The full estimator is *almost globally asymptotically stable*, and locally *exponentially stable*.

6. LEG ODOMETRY

While the tilt of the IMU's frame in the world frame is estimated by the Tilt Observer, its position and yaw are obtained using Leg odometry. Once a contact i is created, its pose is obtained by forward kinematics from the current IMU's frame pose and the robot's joint encoders. This initial pose, which we call the contact's *reference* pose $\left\{\boldsymbol{p}^\star_{\mathcal{C}_i}, \boldsymbol{R}^\star_{\mathcal{C}_i}\right\}$, is considered constant, enforcing the role of fixed anchor of contacts in the world. This pose is then used to recover the pose of the IMU's frame in the world frame. With the proposed pipeline, we thus leverage both the accuracy and mathematical guarantees provided by the Tilt Observer, and the robustness to drift provided by the Leg odometry. Similarly to the computation of the anchor point in Section 4, the contribution of contacts to the Leg odometry is weighted to trust more contacts which are the least prone to slippage, mitigating its effect.

6.1. Estimation of the IMU's orientation in the world

To obtain the yaw from contact information, we compute the weighted average between the reference orientation of the two most reliable contacts[4]. For each contact i, we write:

$$\boldsymbol{R}_{\mathcal{I},i} = \boldsymbol{R}^\star_{\mathcal{C}_i} {}^{\mathcal{C}_i}\boldsymbol{R}_{\mathcal{I}} \tag{21}$$

We then compute the average $\boldsymbol{R}_{\mathcal{I},\text{avg}}$ between both contacts using the formalism defined by SO(3) the Lie group of rotation matrices:

$$\tilde{\boldsymbol{R}} = \boldsymbol{R}^T_{\mathcal{I},1} \boldsymbol{R}_{\mathcal{I},2} \tag{22}$$
$$\boldsymbol{R}_{\mathcal{I},\text{avg}} = \boldsymbol{R}_{\mathcal{I},1} \exp\left(\lambda_2 \text{vec}\left(\log\left(\tilde{\boldsymbol{R}}\right)\right)\right). \tag{23}$$

exp and log are the *exponential* and *logarithm* maps of SO(3). We note that for small angles, we can use the approximation:

$$log\left(\tilde{\boldsymbol{R}}\right) = \frac{1}{2}\left(\tilde{\boldsymbol{R}} - \tilde{\boldsymbol{R}}^T\right), \tag{24}$$

Once the average orientation has been computed, we merge the corresponding yaw with the tilt estimated by the Tilt Observer using the axis agnostic representation introduced in Section 3.

[4] The two contacts with the highest ratio u_i defined in (8)

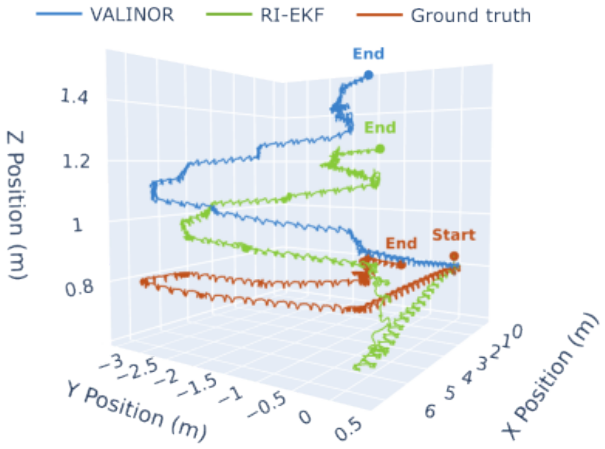

Fig. 3. Tilt

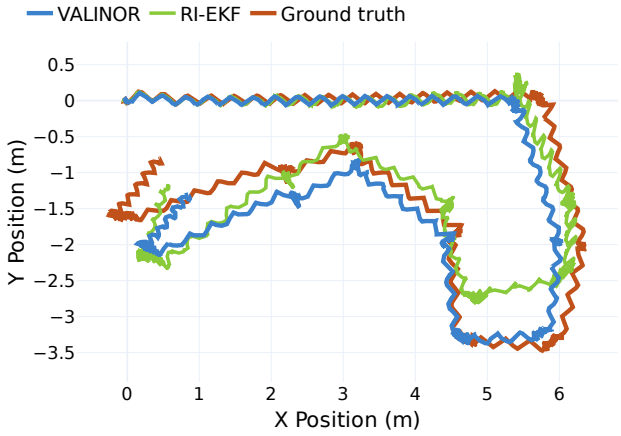

Fig. 4. Tilt

6.2. Estimation of the IMU's position in the world

The position of the IMU's frame in the world frame is obtained from that of the anchor point, which as defined in Section 4 is the point linked to the robot that respects the most the no-slip assumption. Similarly to (10), we compute the anchor point's position in the world frame:

$$\boldsymbol{p}_{\mathcal{A}} = \sum_{i}^{n_c} \lambda_i \boldsymbol{p}^{\star}_{\mathcal{C}_i}, \tag{25}$$

with $\boldsymbol{p}^{\star}_{\mathcal{C}_i}$ the *reference* position of the i-th contact. Using (10) and the newly estimated IMU frame's orientation, we can then compute the IMU's position in the world:

$$\boldsymbol{p}_{\mathcal{I}} = \boldsymbol{p}_{\mathcal{A}} - \boldsymbol{R}_{\mathcal{I}}{}^{\mathcal{I}}\boldsymbol{p}_{\mathcal{A}}. \tag{26}$$

Our position estimate thus also benefitiates from the accurate tilt estimate provided by the Tilt Observer.

7. EXPERIMENTAL EVALUATION

The proposed estimator has been evaluated accross two experimental scenarios on two different humanoid robots[5]:

- a walk on a flat ground over about 18 meters with the robot RHP Friends [32]. This experiment was repeated 5 times, for a total distance of about 90 meters.
- a multi-contact motion over about 2 meters with the robot HRP-5P [33]. This motion involved an additional contact at the robot's left hand, and contacts on tilted obstacles. This experiments was repeated 4 times for a total distance of about 8 meters.

We compare VALINOR, our proposed estimator, with the Right-Invariant EKF (RI-EKF) by [27]. For a fair comparison, both estimators received the same contact state information, from a Schmitt Trigger on the Ground Reaction Force (with thresholds set to 10% and 15% of the robot's weight). Ground truth pose is provided by a motion capture system (OptiTrack, 16 Prime^{X} with 13 cameras), and the ground truth velocity is obtained by finite differences from the ground truth position then filtered with a zero-phase low-pass filter.

The odometry performance of VALINOR and the RI-EKF is evaluated against the ground truth trajectory using the Relative Error (RE), as defined in [34]. RE evaluates the estimation drift over segments of fixed distances. It is particularly relevant for proprioceptive odometry, as it is not affected by global drift, which is unavoidable without exteroceptive sensors. RE therefore provides valuable and easily interpretable insight into the expected local accuracy of the estimator over a given distance.

We compute the Relative Error for lateral $(\boldsymbol{x},\boldsymbol{y})$ and vertical $(\boldsymbol{z})$ translations separately, since these components are generally influenced by different factors. Accuracy in lateral translation would mainly rely on that of local displacements and of yaw estimation, whereas accuracy in vertical translations would be affected by the accuracy of the estimation of the vertical local displacement, of the tilt, and the reliability of the contact height initialization. Similarily, angular errors in tilt and yaw are also evaluated independently.

Finally, we also assess the estimation of the IMU's linear velocity in the world. This velocity is expressed in the frame of the IMU such that it is not affected by errors in the orientation estimate. The velocity error is also separated into lateral and vertical components.

7.1. Multi-contact

We evaluated the performances of VALINOR over a multi-contact motion, implying

7.2. Walk on flat floor

Show table and plot of pose and vel. Focus on tilt.

We can see from Table 2 that the yaw estimation made by the RI-EKF is slightly better than that of VALINOR.

[5]We used the dataset built to evaluate the Kinetics Observer in [28]

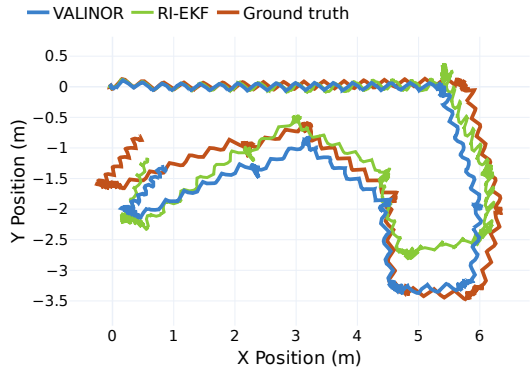

(a) Top view

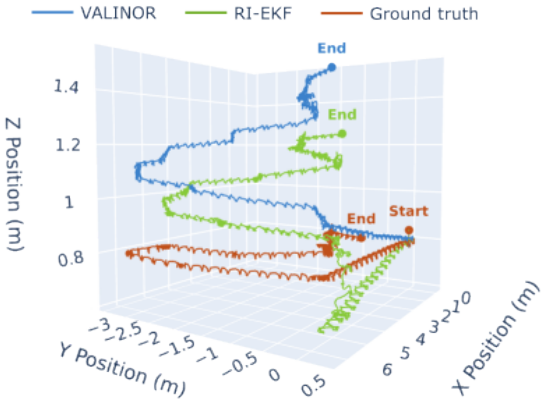

(b) Side view

Fig. 5. Combined figure with two views

We explain this by the fact this orientation comes only from

7.3. Computation times comparison

To prove the computation speed performance of VALINOR, we compared its average computation time per iteration over the four multi-contact experiments, to that of the RI-EKF. In average, an iteration of VALINOR was computed in 2.547 µs, against 19.315 µs for the RI-EKF. The proposed method is thus more than 7.5 times faster than the state-of-the-art estimator, while presenting superior or equivalent accuracy on the target variables.

8. CONCLUSION

Opening: include a correction of the contact pose references. Gyrometer and accelerometer biases.

APPENDIX A

The author(s) can insert an appendix with a meaningful title here.

DECLARATIONS

Conflict of Interest

Always applicable and includes interests of a financial or personal nature. For example, "The authors declare that there is no competing financial interest or personal relationship that could have appeared to influence the work reported in this paper."

Authors' Contributions

If there is one more author, please ensure that all authors' contributions are individually mentioned with their full names.

Table 1. Mean and standard deviation (in parentheses) of errors computed during multi-contact motions. The 0.3 m Relative Error is represented. The best results for each metric are highlighted in bold.

	RE Translation [m]		RE Orientation [°]		Linear velocity [m.s^{-1}]	
	Lateral $\{x, y\}$	Vertical z	Tilt {roll, pitch}	Yaw	Lateral $\{x, y\}$	Vertical z
VALINOR (Proposed)	**0.007** (**0.005**)	**0.002** (**0.003**)	**0.23** (**0.17**)	**0.40** (**0.32**)	0.018 (0.018)	**0.006** (**0.010**)
RI-EKF [27]	0.012 (0.016)	0.004 (0.007)	0.57 (1.02)	0.47 (0.65)	0.015 (0.015)	0.006 (0.009)

Table 2. Mean and standard deviation (in parentheses) of errors computed during the flat odometry. The 1 m Relative Error is represented. The best results for each metric are highlighted in bold.

	RE Translation [m]		RE Orientation [°]		Linear velocity [m.s^{-1}]	
	Lateral $\{x, y\}$	Vertical z	Tilt {roll, pitch}	Yaw	Lateral $\{x, y\}$	Vertical z
VALINOR (Proposed)	**0.031** (**0.021**)	**0.030** (**0.046**)	**0.99** (**1.96**)	1.15 (1.18)	0.018 (0.018)	0.006 (0.010)
RI-EKF [27]	0.047 (0.056)	0.026 (0.051)	1.02 (1.84)	**0.96** (**0.91**)	**0.015** (**0.015**)	0.006 (**0.009**)

Funding

It should be provided in the Declarations, separate from the Acknowledgements. If any of these declarations listed are not relevant to the content of your submission, please state that this declaration is "Not Applicable".

REFERENCES

[1] S. Kuindersma, R. Deits, M. Fallon, A. Valenzuela, H. Dai, F. Permenter, T. Koolen, P. Marion, and R. Tedrake. "Optimization-based locomotion planning, estimation, and control design for the atlas humanoid robot." *Autonomous Robots*, vol. 40, 07 2015.

[2] T. Sugihara and M. Morisawa. "A survey: dynamics of humanoid robots." *Advanced Robotics*, vol. 34, no. 21-22, pp. 1338–1352, 2020.

[3] B. Weng, G. A. Castillo, W. Zhang, and A. Hereid. "On safety testing, validation, and characterization with scenario-sampling: A case study of legged robots." *2022 IEEE/RSJ International Conference on Intelligent Robots and Systems (IROS)*, pp. 5179–5186, 2022.

[4] S. Katayama, M. Murooka, and Y. T. and. "Model predictive control of legged and humanoid robots: models and algorithms." *Advanced Robotics*, vol. 37, no. 5, pp. 298–315, 2023.

[5] E. Dantec, M. Naveau, P. Fernbach, N. Villa, G. Saurel, O. Stasse, M. Taix, and N. Mansard. "Whole-body model predictive control for biped locomotion on a torque-controlled humanoid robot." In *2022 IEEE-RAS 21st International Conference on Humanoid Robots (Humanoids)*, pp. 638–644. Nov 2022. ISSN 2164-0580.

[6] A. Dallard, M. Benallegue, N. Scianca, F. Kanehiro, and A. Kheddar. "Robust Bipedal Walking with Closed-Loop MPC: Adios Stabilizers.", February 2024. URL `https://hal.science/hal-04147602`. Media material :https://youtu.be/hfg7dTpuqu4.

[7] J. Peters, S. Vijayakumar, and S. Schaal. "Reinforcement learning for humanoid robotics." *Proceedings of the third IEEE-RAS international conference on humanoid robots*, pp. 1–20, 01 2003.

[8] Z. Li, X. B. Peng, P. Abbeel, S. Levine, G. Berseth, and K. Sreenath. "Reinforcement learning for versatile, dynamic, and robust bipedal locomotion control." *The International Journal of Robotics Research*, vol. 44, no. 5, pp. 840–888, 2025.

[9] NVIDIA, :, J. Bjorck, F. Castañeda, N. Cherniadev, X. Da, R. Ding, L. J. Fan, Y. Fang, D. Fox, F. Hu, S. Huang, J. Jang, Z. Jiang, J. Kautz, K. Kundalia, L. Lao, Z. Li, Z. Lin, K. Lin, G. Liu, E. Llontop, L. Magne, A. Mandlekar, A. Narayan, S. Nasiriany, S. Reed, Y. L. Tan, G. Wang, Z. Wang, J. Wang, Q. Wang, J. Xiang, Y. Xie, Y. Xu, Z. Xu, S. Ye, Z. Yu, A. Zhang, H. Zhang, Y. Zhao, R. Zheng, and Y. Zhu. "Gr00t n1: An open foundation model for generalist humanoid robots.", 2025. URL `https://arxiv.org/abs/2503.14734`.

[10] K. Kawaharazuka, T. Matsushima, A. Gambardella, J. Guo, C. Paxton, and A. Zeng. "Real-world robot applications of foundation models: A review." *Advanced Robotics*, vol. 38, no. 18, pp. 1232–1254, 2024.

[11] M. N. Zeilinger, D. M. Raimondo, A. Domahidi, M. Morari, and C. N. Jones. "On real-time robust model predictive control." *Automatica*, vol. 50, no. 3, pp. 683–694, 2014. ISSN 0005-1098.

[12] R. Findeisen and F. Allgöwer. "Computational delay in nonlinear model predictive control." *IFAC Proceedings Volumes*, vol. 37, no. 1, pp. 427–432, 2004.

[13] P. Thodoroff, W. Li, and N. D. Lawrence. "Benchmarking real-time reinforcement learning." In *NeurIPS 2021 Workshop on Pre-registration in Machine Learning*, volume 181 of *Proceedings of Machine Learning Research*, pp. 26–41. PMLR, 13 Dec 2022.

[14] R. Firoozi, J. Tucker, S. Tian, A. Majumdar, J. Sun, W. Liu, Y. Zhu, S. Song, A. Kapoor, K. Hausman, B. Ichter, D. Driess, J. Wu, C. Lu, and M. Schwager. "Foundation models in robotics: Applications, challenges, and the future." *The International Journal of Robotics Research*, vol. 44, no. 5, pp. 701–739, 2025.

[15] D. Wisth, M. Camurri, and M. Fallon. "Vilens: Visual, inertial, lidar, and leg odometry for all-terrain legged robots." *IEEE Transactions on Robotics*, vol. 39, no. 1, pp. 309–326, 2022.

[16] M. Fallon. "Accurate and robust localization for walking robots fusing kinematics, inertial, vision and lidar." *Interface focus*, vol. 8, no. 4, pp. 20180015, 2018.

[17] Y. Kuang, T. Hu, M. Ouyang, Y. Yang, and X. Zhang. "Tightly coupled lidar/imu/uwb fusion via resilient factor graph for quadruped robot positioning." *Remote Sensing*, vol. 16, no. 22, 2024. ISSN 2072-4292.

[18] P.-C. Lin, H. Komsuoglu, and D. Koditschek. "A leg configuration measurement system for full-body pose estimates in a hexapod robot." *IEEE Transactions on Robotics*, vol. 21, no. 3, pp. 411–422, June 2005. ISSN 1941-0468.

[19] M. Bloesch, M. Hutter, M. A. Hoepflinger, S. Leutenegger, C. Gehring, C. D. Remy, and R. Siegwart. "State estimation for legged robots-consistent fusion of leg kinematics and IMU." *Robotics*, vol. 17, pp. 17–24, 2013.

[20] P. Wawrzyński, J. Możaryn, and J. Klimaszewski. "Robust estimation of walking robots velocity and tilt using proprioceptive sensors data fusion." *Robotics and Autonomous Systems*, vol. 66, pp. 44–54, 2015. ISSN 0921-8890.

[21] K. Masuya and T. Sugihara. "Dead reckoning for biped robots that suffers less from foot contact condition based on anchoring pivot estimation." *Advanced Robotics*, vol. 29, no. 12, pp. 785–799, 2015.

[22] M. Benallegue, R. Cisneros, A. Benallegue, Y. Chitour, M. Morisawa, and F. Kanehiro. "Lyapunov-Stable Orientation Estimator for Humanoid Robots." *IEEE Robotics and Automation Letters*, vol. 5, no. 4, pp. 6371–6378, October 2020.

[23] R. Mahony, T. Hamel, and J.-M. Pflimlin. "Nonlinear complementary filters on the special orthogonal group." *IEEE Transactions on automatic control*, vol. 53, no. 5, pp. 1203–1218, 2008.

[24] T.-Y. Lin, R. Zhang, J. Yu, and M. Ghaffari. "Legged robot state estimation using invariant kalman filtering and learned contact events." In A. Faust, D. Hsu, and G. Neumann, editors, *Proceedings of the 5th Conference on Robot Learning*, volume 164 of *Proceedings of Machine Learning Research*, pp. 1057–1066. PMLR, 08–11 Nov 2022.

[25] M. Maravgakis, D.-E. Argiropoulos, S. Piperakis, and P. Trahanias. "Probabilistic contact state estimation for legged robots using inertial information." In *2023 IEEE International Conference on Robotics and Automation (ICRA)*, pp. 12163–12169. IEEE, 2023.

[26] Z. Yoon, J.-H. Kim, and H.-W. Park. "Invariant smoother for legged robot state estimation with dynamic contact event information." *IEEE Transactions on Robotics*, 2023.

[27] R. Hartley, M. Ghaffari, R. M. Eustice, and J. W. Grizzle. "Contact-aided invariant extended kalman filtering for robot state estimation." *The International Journal of Robotics Research*, vol. 39, no. 4, pp. 402–430, 2020.

[28] A. Demont, M. Benallegue, A. Benallegue, P. Gergondet, A. Dallard, R. Cisneros, M. Murooka, and F. Kanehiro. "The Kinetics Observer: A Tightly Coupled Estimator for Legged Robots.", December 2024. URL `https://hal.science/hal-04616647`. Working paper or preprint.

[29] R. Grandia, E. Knoop, M. Hopkins, G. Wiedebach, J. Bishop, S. Pickles, D. Müller, and M. Bächer. "Design and control of a bipedal robotic character." In *Robotics: Science and Systems XX*, RSS2024. Robotics: Science and Systems Foundation, July 2024.

[30] M. Tsuru, A. Escande, I. Kumagai, M. Murooka, and K. Harada. "Online multi-contact motion replanning for humanoid robots with semantic 3d voxel mapping: Exoctomap." *Sensors*, vol. 23, no. 21, 2023. ISSN 1424-8220.

[31] P. Martin, I. Sarras, M.-D. Hua, and T. Hamel. "A global exponential observer for velocity-aided attitude estimation.", 2016. URL `https://arxiv.org/abs/1608.07450`.

[32] M. Benallegue, G. Lorthioir, A. Dallard, R. Cisneros-Limón, I. Kumagai, M. Morisawa, H. Kaminaga, M. Murooka, A. Andre, P. Gergondet, K. Kaneko, G. Caron, F. Kanehiro, A. Kheddar, S. Yukizaki, J. Karasuyama, J. Murakami, and M. Kamon. "Humanoid robot rhp friends: Seamless combination of autonomous and teleoperated tasks in a nursing context." *IEEE Robotics and Automation Magazine*, vol. 32, no. 1, pp. 79–90, March 2025. ISSN 1558-223X.

[33] K. Kaneko, H. Kaminaga, T. Sakaguchi, S. Kajita, M. Morisawa, I. Kumagai, and F. Kanehiro. "Humanoid robot hrp-5p: An electrically actuated humanoid robot with high-power and wide-range joints." *IEEE Robotics and Automation Letters*, vol. 4, no. 2, pp. 1431–1438, April 2019. ISSN 2377-3766.

[34] Z. Zhang and D. Scaramuzza. "A tutorial on quantitative trajectory evaluation for visual(-inertial) odometry." In *2018 IEEE/RSJ International Conference on Intelligent Robots and Systems (IROS)*, pp. 7244–7251. Oct 2018. ISSN 2153-0866.